Journal of Marine Science and Engineering

MDPI

Article

Experimental and Numerical Study on Influence of Wheel Attachments on Resistance Performance of Amphibious Vessel for Marine Debris Collection

Won-June Jeong [1], Seol Nam [1], Jong-Chun Park [1,*] and Hyeon Kyu Yoon [2]

[1] Department of Naval Architecture and Ocean Engineering, Pusan National University, Busan 46241, Republic of Korea; myj8888e@pusan.ac.kr (W.-J.J.); stdq0201@pusan.ac.kr (S.N.)
[2] Department of Naval Architecture and Ocean Engineering, Changwon National University, Changwon 51140, Republic of Korea; hkyoon@changwon.ac.kr
* Correspondence: jcpark@pnu.edu

Abstract: This study aims to investigate the influence of wheel configurations on hydrodynamic resistance of an amphibious vessel through experiments and simulations. To evaluate the resistance performance associated with wheel attachments, three configurations were examined: vessel without attachments, with caterpillars, and with both caterpillars and shoe−paddles. A comprehensive series of computational fluid dynamics (CFD) simulations were conducted for these attachment types, complemented by experimental validations. The Volume-of-Fluid (VOF) model was employed in CFD simulations to capture the free surface movement, and the Dynamic Fluid–Body Interaction (DFBI) model was adopted to represent the two-degree-of-freedom motion of the vessel, specifically trim and sinkage. The total resistance derived from CFD simulations was calculated across a range of Froude numbers (Fns), including the design speed of the target vessel, and validated through model tests conducted in a wave basin equipped with a towing facility. The analysis indicated a general increase in resistance when attachments were added to the amphibious vessel. Remarkably, at the design speed (Fn = 0.27), the total resistance with both caterpillars and shoe−paddles exceeded that of the configuration without any attachments by more than 75.7%. These results provide crucial insights for the preliminary design stage of amphibious vessels, particularly those intended for marine debris collection in hard-to-reach areas.

Keywords: amphibious vessel; resistance performance; trim and sinkage; caterpillars; shoe−paddles; computational fluid dynamics (CFD); experiment

Citation: Jeong, W.-J.; Nam, S.; Park, J.-C.; Yoon, H.-K. Experimental and Numerical Study on Influence of Wheel Attachments on Resistance Performance of Amphibious Vessel for Marine Debris Collection. *J. Mar. Sci. Eng.* **2024**, *12*, 570. https://doi.org/10.3390/jmse12040570

Academic Editor: Rafael Morales

Received: 24 February 2024
Revised: 21 March 2024
Accepted: 27 March 2024
Published: 27 March 2024

1. Introduction

Debris washed into the ocean by typhoons and winds or waves can damage coastal landscapes and severely impact marine ecosystems and habitats. The international community has long been concerned about and active in protecting the marine environment. Specifically, the United Nations Environment Assembly (UNEA) has issued annual resolutions since 2014 to identify the origins of plastic debris entering the ocean and to pinpoint technologies and practices for minimizing its entry [1]. Recently, it has intensified its efforts to prevent and reduce marine debris by issuing a resolution calling for the establishment of a relevant expert organization and binding measures by 2025. Meanwhile, 14 major ports in South Korea are also making various efforts to reduce marine debris, including operation of cleaning vessels. However, collecting debris in coastal areas, such as rocky coasts or uninhabited islands, remains challenging due to the difficulty of cleaning vessels to reach these areas, exacerbated by wind or waves. To address this problem, the construction of amphibious marine debris collection vessels, capable of operating in inaccessible coastal and offshore areas, has been proposed. An amphibious vessel,

designed as a catamaran, features caterpillars with several wheels connected to both hulls and a shoe-paddle attached to the top of the caterpillar, propelling the vessel forward through its rotation.

In this context, research involving experiments or numerical simulations on the resistance of amphibious vehicles has recently been undertaken. Nakisa et al. [2] used computational fluid dynamics (CFD) to compare the drag of a multipurpose amphibious vehicle in finite and infinite water depths. Yamashita et al. [3] aimed to propose a methodology for simulating amphibious vessels transitioning between land and water modes. Sun et al. [4] and Pan et al. [5] conducted studies using experiments and simulations to improve resistance performance by adding flaps as attachments to reduce lateral resistance of high-speed amphibious vehicles. Liu et al. [6] performed optimal design using CFD by selecting and analyzing shape control parameters as optimal design variables to reduce the hydrodynamic resistance of an amphibious vehicle, comparing the results with experiments. Jaouad et al. [7] also focused on using CFD for amphibious vehicles to minimize drag and improve the aerodynamic performance characteristics of these vehicles. More et al. [8] conducted model testing and CFD simulation to estimate the resistance of amphibious vehicles in relation to their surface characteristics, concluding that a smoother surface results in reduced viscous resistance. Guo et al. [9] and Pan et al. [10] used numerical simulation to predict the pressure distribution and free-surface elevation on the surface of the amphibious vehicle during navigation. Du et al. [11] examined the primary parameters affecting the resistance performance of amphibious vehicles. Their research identified crucial parameters that influence the resistance characteristics of these vessels, such as the length-to-draught ratio, length-based Froude number, volume-based Froude number, block coefficient, volume–length coefficient, loss of waterplane area, and trim angle. Behara et al. [12] studied the hydrodynamic characteristics of a waterjet-propelled amphibious craft traveling in displacement and planning modes via full-scale experiments and numerical simulations. Lee et al. [13] conducted an experiment to improve the forward ability of a high-speed military amphibious vehicle while moving at sea and to predict trim and sinkage.

Although research on amphibious vehicles has been continuously conducted in various fields, comparative studies on resistance according to the shape of the wheels of amphibious vehicles are limited. Recently, Dhana et al. [14] investigated the resistance performance of amphibious vehicles, focusing on the effects of the hull designs and caterpillar tracks through both experimental and CFD simulations. This paper seeks to build upon the work of Dhana et al. [14] by evaluating the resistance performance when shoe-paddle attachments are added to the caterpillars. Specifically, this study aims to assess the impact of wheel attachments on resistance performance by analyzing the resistance components, wave patterns, and running trim across different vessel speeds. By juxtaposing experimental and CFD simulation results, we aim to scrutinize the influence of wheel attachments on the resistance of amphibious vehicles. Whereas previous study primarily concentrated on the presence or absence of caterpillars, the present study introduces shoe-paddle attachments to perform experiments under more intricate conditions, thereby aiming for a comprehensive understanding of how various attachments affect the resistance performance of amphibious vehicles. For reference, since the purpose of the amphibious vehicle is marine debris collection, it is henceforth defined as an 'amphibious vessel' in this study.

2. Numerical Simulation

2.1. Target Model

In this study, CFD analysis was conducted at model scale, consistent with the experimental setup. Three types of models were used for both experimental and CFD analysis, as depicted in Figure 1. Model (a) represents the bare hull of the basic model, similar to a catamaran. Model (b) illustrates the same model with a wheel-shaped caterpillar attached

to the bare hull. And model (c) depicts the amphibious vessel with shoe−paddles attached outside the caterpillars, enhancing structural stability for land movement. Table 1 provides the principal dimensions of the full-scale amphibious vessel. This vessel is relatively small, with a length of 10.767 m, and is symmetrical about the centerline. The weights of the caterpillars and paddles are considered negligible in comparison to the overall weight of the vessel. CFD simulations were performed using a 1/10.767 scale model to validate the experimental results.

Table 1. Principal dimensions of the amphibious vehicle.

Principal Dimension	Full-Scale
Length overall, LOA (m)	10.767
Waterline length, LWL (m)	9.253
Breadth, B (m)	3.800
Draft, T (m)	0.750
Displacement weight, W (kgf)	14,493.830
Longitudinal center of gravity, LCG from AP (m)	4.978
Vertical center of gravity, VCG from BL (m)	0.399
Kxx/B (-)	0.400
Kyy/L (-)	0.250
Kzz/L (-)	0.250
Design speed, U (m.s^-1)	2.778

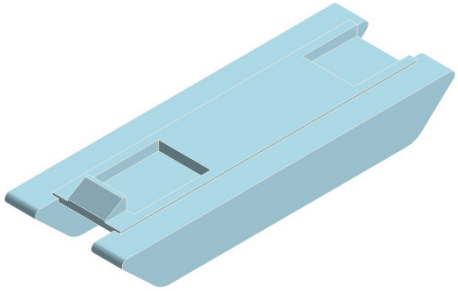

(**a**)

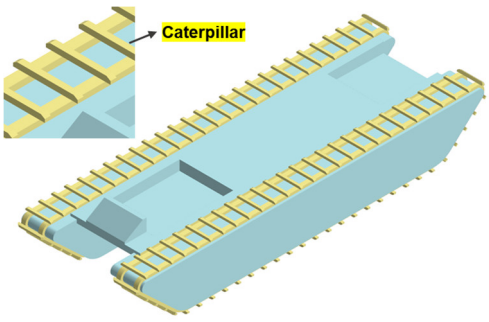

(**b**)

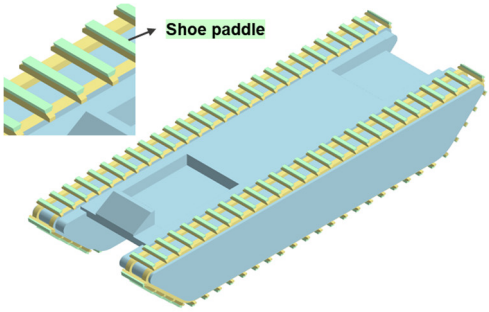

(**c**)

Figure 1. Model of amphibious vessels. (**a**) Bare hull. (**b**) With caterpillar. (**c**) With caterpillars and shoe−paddles.

2.2. Governing Equations

In this study, the flow field around an amphibious vessel considering its running trim was simulated, and it varies depending on whether caterpillars and paddles are attached or absent. The simulation was conducted using the commercial CFD software STAR-CCM+ version 16.04. The governing equations employed were the continuity and momentum equations, and unsteady Reynolds-averaged Navier–Stokes (URaNS) simulations were performed.

$$\frac{\partial u_i}{\partial x_i} = 0 \tag{1}$$

$$\frac{\partial u_i}{\partial \mathrm{t}} + u_j \frac{\partial u_i}{\partial x_j} = -\frac{1}{\rho}\frac{\partial \rho}{\partial x_i} + \frac{\partial}{\partial x_j}\left[\nu\left(\frac{\partial u_i}{\partial x_j} + \frac{\partial u_i}{\partial x_i}\right) - \overline{u'_i u'_j}\right] + g_i \tag{2}$$

where u is the total velocity vector, x is the position vector, t is the time, ρ is the density, p is the pressure, v is the kinematic viscosity, g is the gravitational acceleration, and $\overline{u'_i u'_j}$ is the Reynolds stress.

2.3. Numerical Implementation

The governing equations mentioned in Section 2.2 are discretized by a Finite-Volume method (FVM), with the diffusion and convection terms being solved by the second-order central scheme and the first-order upwind scheme, respectively. For pressure–velocity coupling, the SIMPLE algorithm (Semi-Implicit Method for Pressure-Linked Equations) was employed. For the turbulence model, the Shear Stress Transport (SST) $k-\omega$ model, based on the two-equation model and used in Dhana et al. [14], was employed. Furthermore, the Volume-of-Fluid (VOF) model [15] was adopted to capture the location of the free surface.

To represent the running trim, such as sinkage and trim of the vessel, the Dynamic Fluid–Body Interaction (DFBI) model [16] was introduced. This model calculates the responses of the target object to the hydrodynamic forces and moments applied by the physical continuum. Hydrodynamic forces and moments acting on the hull are determined through a CFD simulation of the flow field. Subsequently, the new position of the hull can be established by solving a two-degree-of-freedom (2-DOF) model of the motion equation independently. In this study, a 2-DOF motion analysis was conducted, specifically activating the heave (translational motion in the z-direction) and pitch (rotational motion in the y-direction), as illustrated in Figure 2.

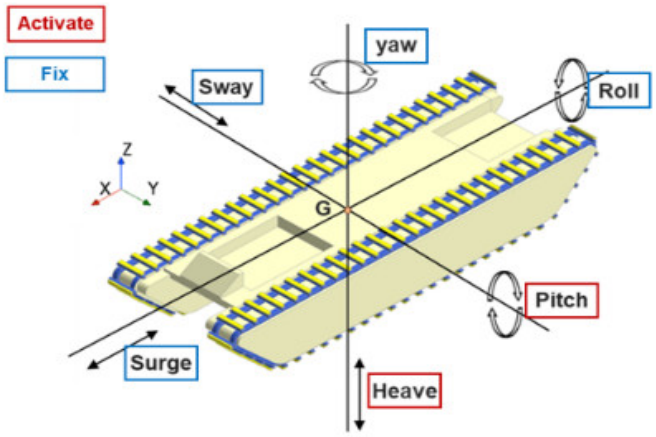

Figure 2. Schematic view of implementing 2-degree-of-freedom motion.

2.4. Boundary Conditions and Mesh Generation

Referring to the International Towing Tank Conference (ITTC) ship resistance CFD guidelines [17], the size of the virtual towing tank was determined, as shown in Figure 3, and the boundary conditions were set as detailed in Table 2. To enhance calculation efficiency, only half of the domain including the hull was analyzed, applying a symmetry boundary condition to the center plane. As depicted in Figure 4, the mesh system was generated using trimmer mesh, a type of unstructured grid. Additionally, 12 prism layers were implemented on the surface to account for the viscous effects on the hull surface. With a total of approximately 2.3 million grids, a base grid size of 0.0177 m was used. The intricate designs of the caterpillar tracks and shoe−paddles led to relatively high y+ values ($y+ < 50$) around the wheel surface. Additionally, for wall treatment, an enhanced wall function that combines both linear and logarithmic standard laws was utilized. The time step (dt) is dynamically adjusted to keep the Courant number below 1 during the simulation, ensuring the reliability and accuracy of the results. The initial time step was established at dt = 0.002 s.

To ensure the reliability of the numerical simulation, the Grid Convergence Index (GCI) was calculated through a grid convergence test. The GCI is a metric used for grading determination, calculating the convergence error of the grid based on Richardson's extrapolation [18]. In this simulation, five different grid sizes ranging from G1 to G5 were configured, as shown in Figure 5. The GCI calculations were performed using the procedure proposed by [19,20]. The results, graphed in Figure 6, indicate that the total resistance tends to converge to a constant value as the mesh density increases. To quantitatively evaluate these values, the GCI was calculated using three mesh levels, as shown in Table 3. Here, the refinement factor, r, is 1.414, representing the ratio of the grid size, and p represents the formal order of accuracy of the algorithm. GCI_f and GCI_c imply the percentage of asymptotic solutions derived with the fine and coarse mesh, respectively, with error values indicating their deviation from the asymptotic value. R is the convergence ratio, considered convergent if it falls between 0 and 1, and divergent if greater than 1. Through the GCI calculation, G4 was selected as the optimal grid size, utilizing about 2.3 million grids with a base size of 0.0177 m.

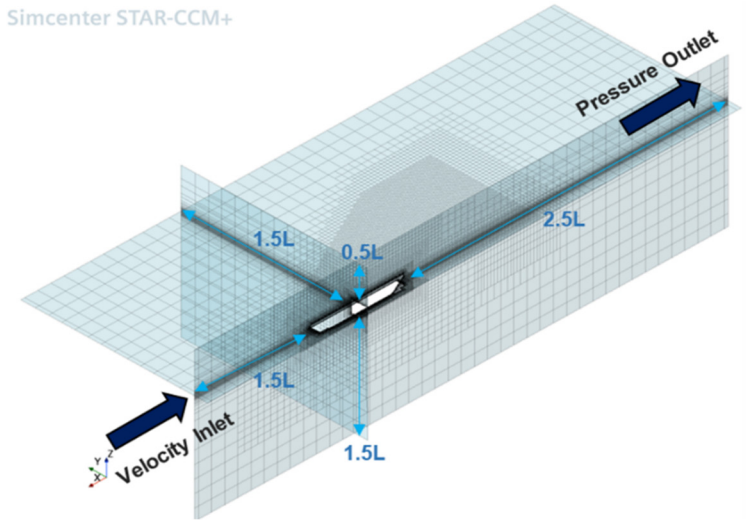

Figure 3. Computational domain of virtual towing tank.

Table 2. Boundary conditions.

Numerical Simulation of Plate	Boundary Conditions
Top, Bottom, and Inlet	Velocity Inlet (Dirichlet condition)
Side & Outlet	Pressure Outlet (Dirichlet and Neuman conditions)
Amphibious vessel (Hull/Caterpillars/Shoe−paddles)	Wall (No-slip condition)
Center-plane	Symmetry

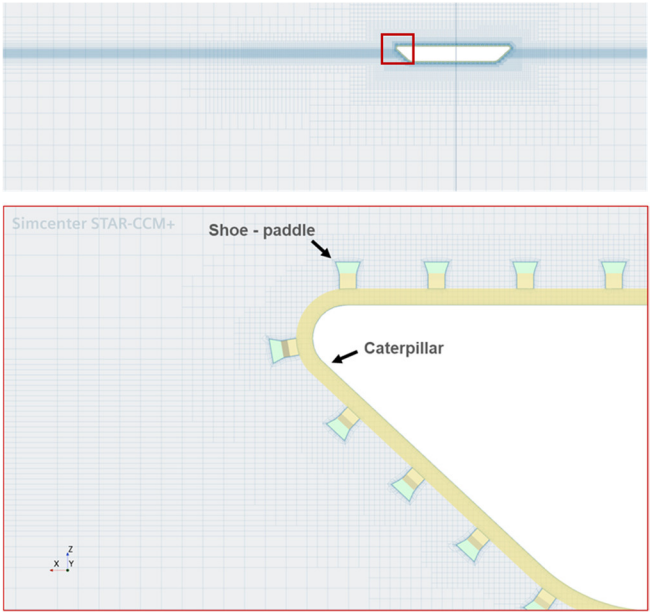

Figure 4. Mesh configuration: example for case with caterpillars and shoe–paddles.

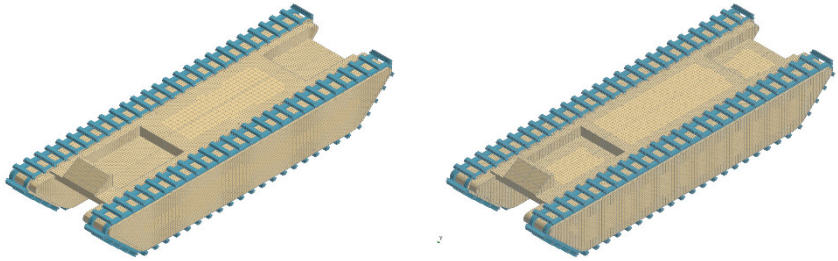

G1 (369,777) G2 (710,267)

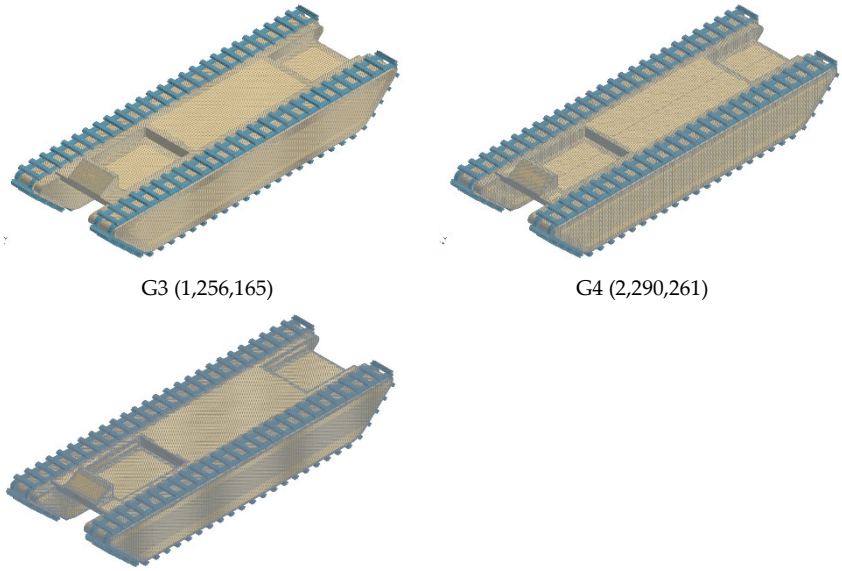

Figure 5. Grid system GCI values by different mesh levels.

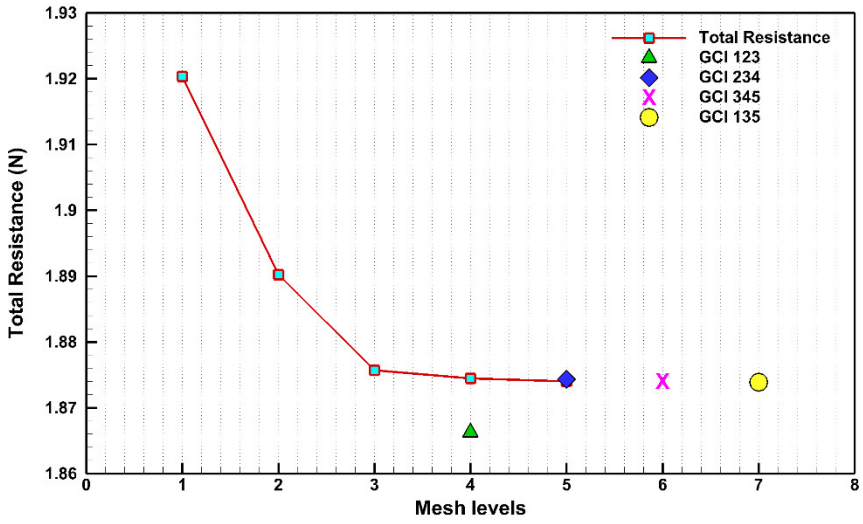

Figure 6. Grid independence index (GCI).

Table 3. Grid convergence index (GCI).

Mesh Level	123	234	345	135
r	1.414	1.414	1.414	2.000
p	2.105	7.179	2.710	4.734
GCI_f	0.901	0.007	0.020	0.004
GCI_c	1.854	0.088	0.052	0.116
R	0.482	0.083	0.391	0.038

3. Results and Discussion

3.1. Experiments for Validation

The experiment was conducted in a physical wave basin with a towing carriage at Changwon National University in Korea to validate the simulation results. A load cell was employed to measure the resistance acting on the hull. The electrical signal from the load cell output was converted into a digital signal through an Analog-to-Digital (A/D)

converter. A clamp system was used to prevent overload of the load cell due to the changing attitudes of the vessel, influenced by the pressure around the hull during the experiment. Particularly, in tests involving caterpillars and shoe–paddles, sinkage and trim were measured to ascertain the vessel's condition under each test scenario. Two potentiometers were attached to the bow and stern of the amphibious vessel model to determine sinkage and trim, adjusting sensitivity and balance by transmitting a portion of the voltage in response to the motion detection sensor.

Figure 7 displays the experimental setup for the resistance test of the amphibious vessel. The model was secured to the frame structure in the middle of a towing carriage. The resistance force acting on the hull was measured through a load cell installed on the vessel and the connection between the frame structure and the vessel. In addition, the model was fixed with a clamp to maintain stability and limit excessive movement during acceleration and deceleration. The experiment was conducted at various speeds in the range of Fn = 0.1 ~ 0.25 to observe the resistance values corresponding to different velocities.

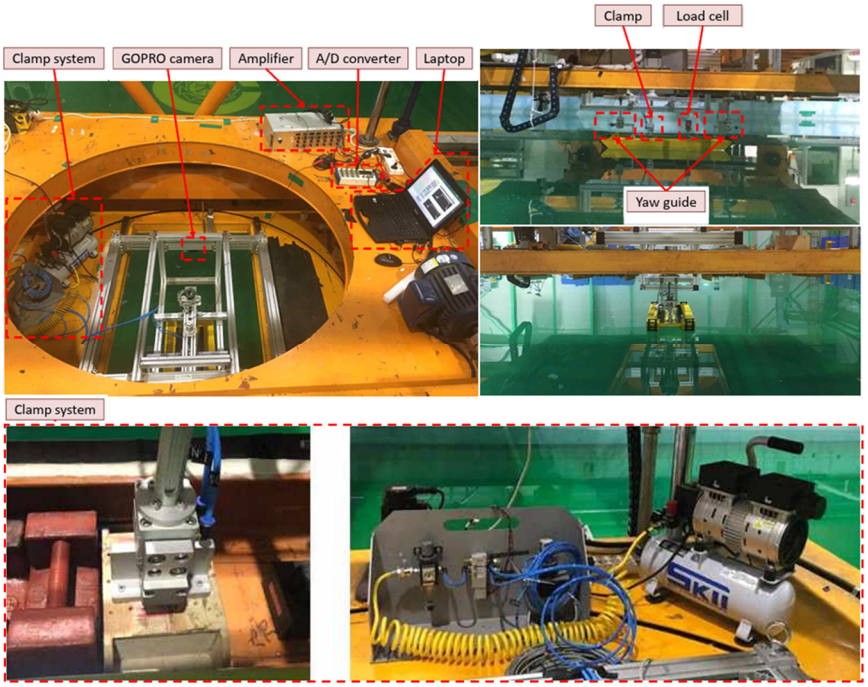

Figure 7. Experimental setup of resistance test for amphibious vessel.

3.2. Validation and Discussion

3.2.1. Effect of Attachments on Total Resistance

The comparison of total resistance as a function of Froud number between the experiment and CFD simulation is shown in the figure. In the model test, the design speed (Fn = 0.27) for the amphibious vessel model could not be achieved due to limitations in the water basin facility. As a result, simple linear regression was employed to estimate the resistance at the design speed. Equations (3)–(5) represent the quadratic trend lines and determination coefficient (R^2) for the case of the bare hull only, for the case with caterpillars, and for the case with both caterpillars and shoe–paddles, respectively. Here, the closer R^2 is to 1, the more accurately the trend line expresses the data tendency. Consequently, it was found that the analysis results, for all three configurations, in a very high correlation according to the trend line.

$$y = 96.302x^2 - 13.442x + 0.9329,\ R^2 = 0.9991 \quad (3)$$

$$y = 83.676x^2 - 10.828x + 0.7260,\ R^2 = 0.9991 \quad (4)$$

$$y = 65.096x^2 - 11.587x + 0.8149,\ R^2 = 0.9987 \quad (5)$$

Figure 8 presents a comparison of total resistance results from both experiments and simulations across various Froude numbers. Upon comparing the results of the model test with those of the CFD simulation, it was concluded that the simulation accuracy remained quite valid, with a relative error range of 0 to 6.56%. In the comparison of CFD simulation results at the design speed based on attachments, the total resistance for the case with both caterpillars and shoe−paddles increased by 75.7% compared to that for the case of the bare hull and by 11.0% compared to that for the case with caterpillars.

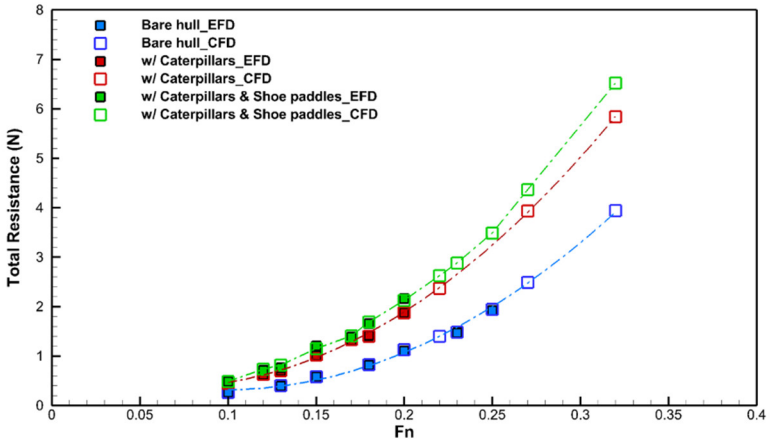

Figure 8. Comparison of total resistance as a function of Froude number between experiment and numerical simulation.

It may be logically consistent that an increase in the attachments leads to a corresponding increase in the projected area, which in turn enhances the overall hydrodynamic resistance. Accordingly, to analyze the resistance characteristics by components, the resistance coefficient, non-dimensionalized relative to the wetted area, was calculated from the total resistance. The total resistance (R_{TM}) was divided into two components, pressure resistance (R_{PM}) and then friction resistance (R_{FM}), and a non-dimensional resistance coefficient was calculated for each component, as described in Equations (6)–(8):

$$C_{TM} = R_{TM}/\rho_M S_M {V_M}^2 \quad (6)$$

$$C_{PM} = R_{PM}/\rho_M S_M {V_M}^2 \quad (7)$$

$$C_{FM} = R_{FM}/\rho_M S_M {V_M}^2 \quad (8)$$

where ρ_M represents the density of fresh water, V_M is the vessel speed, and S_M is the wetted area [21].

Figure 9 shows the resistance coefficients separated by a component as a function of Froude number (Fn).

For this amphibious vessel, it has been observed that the proportion of pressure resistance in the total resistance exceeds that of frictional resistance. At the design speed, it was found that the bare hull exhibited pressure resistance accounting for 84.3% of the total resistance, while the case with caterpillars showed 91.6%, and the case with both caterpillars and shoe−paddles accounted for 92.0%. Moreover, even with an increase in the Fn, the change in frictional resistance was minimal. This indicates that the addition of attachments leads to a significant increase in pressure resistance, which encompasses total pressure, including hydrostatic pressure, especially at the lower hull, as depicted in Figure 10. The reasons for this situation will be discussed in the subsequent Section 3.2.2.

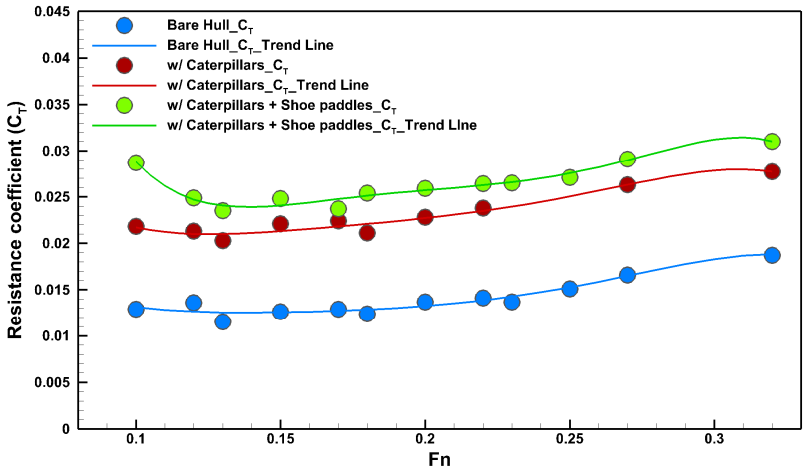

(**a**)

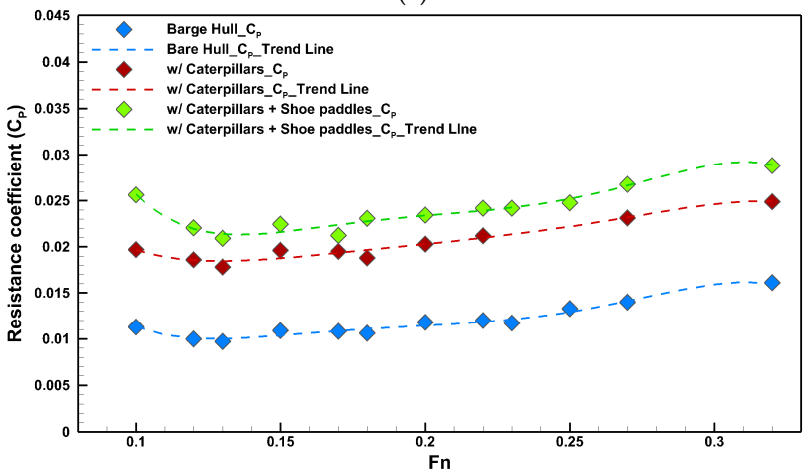

(**b**)

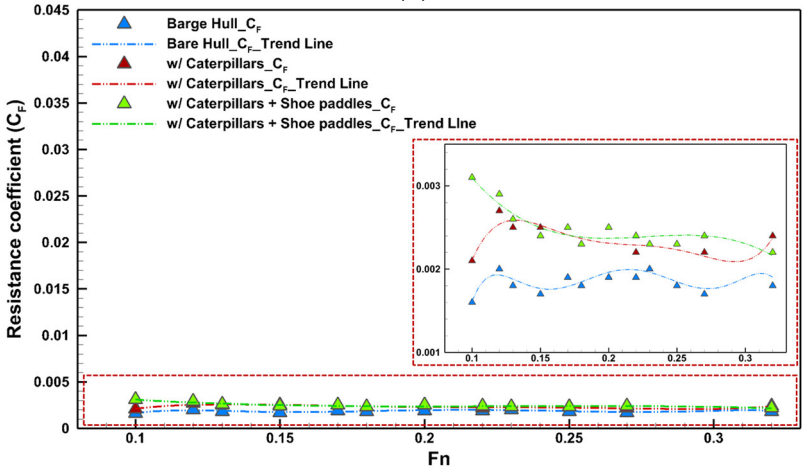

(**c**)

Figure 9. Components of resistance coefficients. (**a**) Total resistance coefficient. (**b**) Pressure resistance coefficient. (**c**) Frictional resistance coefficient.

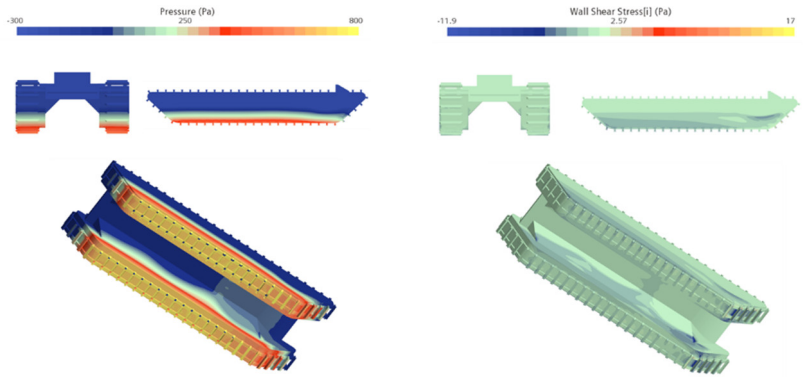

(**a**) (**b**)

Figure 10. Comparison of pressure and shear stress distribution at design speed for case with both caterpillars and shoe−paddles. (**a**) Pressure distribution. (**b**) Shear stress distribution.

As previously discussed, it has been observed that the presence or absence of attachments, such as caterpillars and shoe–paddles, significantly affects the total resistance. Given the total resistance of the vessel, it is now crucial to estimate the effective power for designing the adequate propulsion system.

First, the original ITTC-1957 method from the International Towing Tank Committee (ITTC) was utilized to calculate the resistance coefficient value (C_{TS}) for a full-scale ship. The sequence of equations and processes necessary for this calculation is as follows:

$$C_{RM} = C_{TM} - C_{FM} \tag{9}$$

$$C_{FM} = 0.075/(log_{10}Re_M - 2)^2 \tag{10}$$

$$Re_M = V_M \cdot L_{wlM}/\nu \tag{11}$$

$$C_{RS} = C_{RM} \tag{12}$$

$$C_{TS} = C_{FS} + C_{RM} + C_A \tag{13}$$

$$C_{FS} = 0.075/(log_{10}Re_S - 2)^2 \tag{14}$$

$$Re_S = V_S \cdot L_{wlS}/\nu \tag{15}$$

where C_{RM} is the residual resistance coefficient at model test, C_A is the model–ship correlation allowance coefficient, considered as 0.6×10^{-3} [22], Re is the Reynolds number, and L_{wl} is the waterline length.

Subsequently, the resistance of the full-scale ship (R_{TS}) and effective horsepower (P_E) are determined as follows:

$$R_{TS} = \left(0.5\rho_S S_s {V_s}^2\right) C_{TS} \tag{16}$$

$$P_E = R_{TS} \cdot V_S/745 \tag{17}$$

where ρ_S is the density of sea water.

The estimated results for effective horsepower are depicted in Figure 11. The analysis results reveal that the addition of attachments to the wheels of an amphibious vessel leads to a significant increase in effective horsepower. This suggests that the inclusion of attachments on the hull results in increased resistance, necessitating more power engine operation. When comparing the effective horsepower necessary for the design of the propulsion system at the design speed of 5.4 knots, there is an increase of approximately 66.7% with the addition of only 'caterpillar' to the 'bare hull'. The increase is about 86.5% when both

'caterpillar' and 'shoe−paddles' are added. These results enable the determination of the specifications for engines and auxiliary equipment required to achieve the design speed.

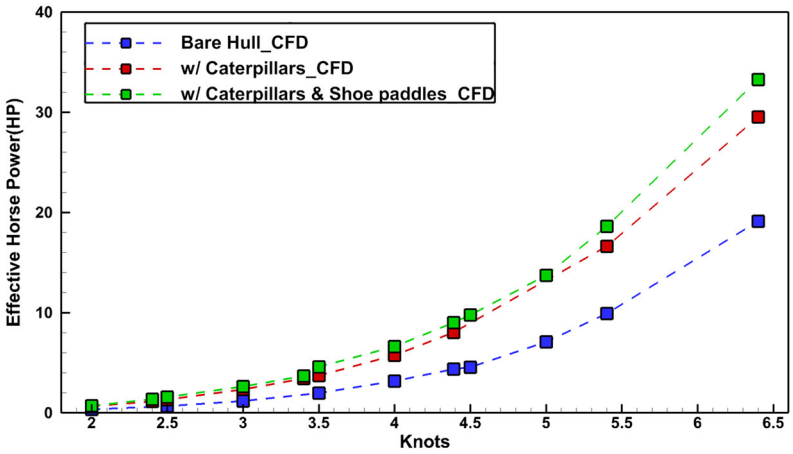

Figure 11. Comparison of effective horsepower according to presence or absence of attachments.

3.2.2. Variation of Wave Patterns

To compare wave patterns at the design speed for the cases with and without attachments, simulation results were analyzed using the flow field data when a quasi-steady state had been reached.

As illustrated in Figure 12, the wave patterns observed demonstrate that the caterpillars and shoe−paddles interact with the original waves generated by the bare hull, dampening the waves adjacent to the hull. This interaction also generates an additional wave system characterized by more divergent and transverse waves that propagate further from the hull. Figure 13 depicts wave profiles around the vessel's bow, highlighting significant changes in the wave profiles near the bow due to the added attachments. These changes seem likely to be attributable to intensified energy dissipation mechanisms, as the bow wave-breaking phenomena, engendered by the attachment–fluid interaction, become more pronounced with additional attachments. Consequently, the resistance encountered by the hull with additional appendages increases due to wave breaking near the bow. This increase in energy dissipation during the wave-breaking process subsequently dampens the development of the wave profile along the hull towards the stern, as demonstrated in Figure 14. Such observations can elucidate the diminution of wave propagation in the wake region at the stern of the hull, as depicted in Figure 12, correlating it with the effects induced by the increased attachments and the consequent energy dissipation dynamics.

To summarize, the introduction of attachments inhibits the development of wave patterns along the hull due to heightened energy dissipation during breaking waves near the hull, thereby contributing to increased wave-breaking resistance. Nevertheless, it is posited that the wave patterns developing farther from the hull, originally generated by the bare hull, are accentuated due to the slightly enlarged cross-sectional area of the appendages, leading to an increase in wave-making resistance.

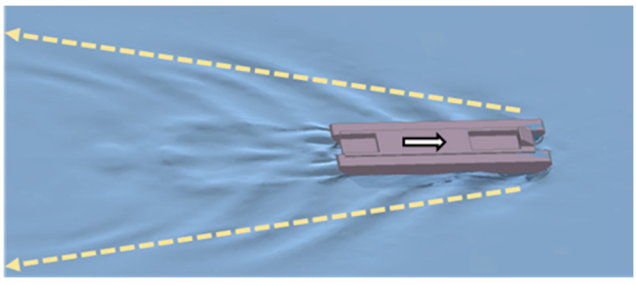

(**a**)

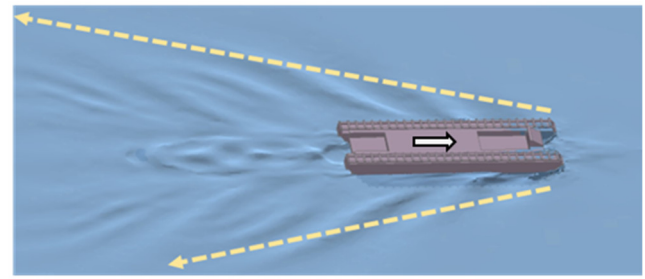

(**b**)

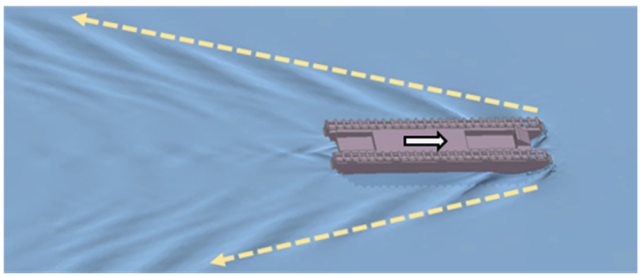

(**c**)

Figure 12. Wave configuration around amphibious vessel at design speed. (**a**) Bare hull. (**b**) With caterpillars. (**c**) With caterpillars and shoe−paddles.

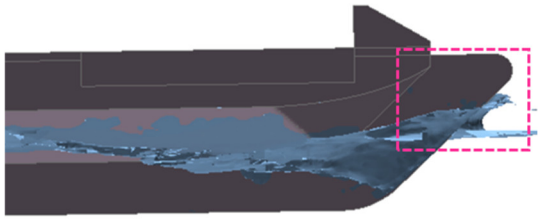

(**a**)

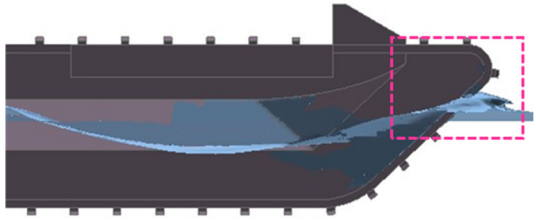

(**b**)

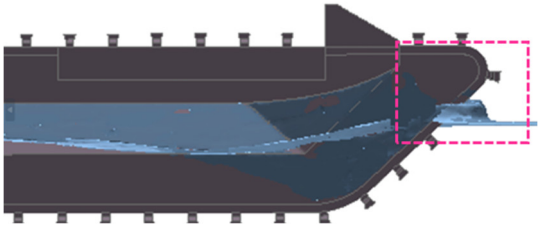

(**c**)

Figure 13. Wave configuration around bow of amphibious vessel at design speed. (**a**) Bare hull. (**b**) With caterpillars. (**c**) With caterpillars and shoe−paddles.

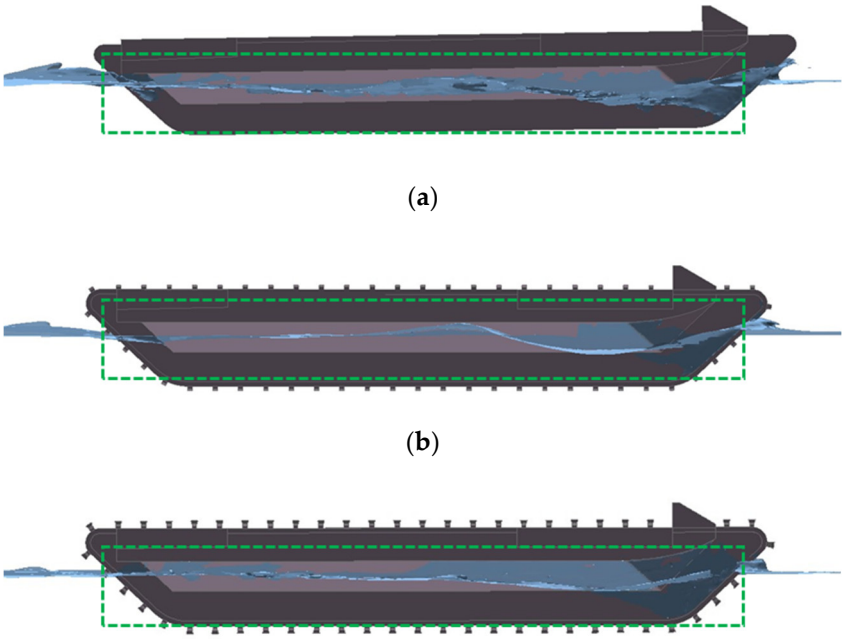

(**a**)

(**b**)

(**c**)

Figure 14. Wave profiles along hull at design speed. (**a**) Bare hull. (**b**) With caterpillars. (**c**) With caterpillars and shoe−paddles.

3.2.3. Changes in Running Trim

CFD simulations were performed to analyze changes in the running trim of a vessel, with results compared with model test results. Notably, the experimental phase was confined to a scenario incorporating all attachments separately.

Figures 15 and 16 depict the variations in trim and sinkage with respect to the Fn, respectively. Initially, the trim analysis for the bare hull shows minimal variation across a range of Fns. However, the equipment of caterpillar tracks results in a slight increase in stern trim as Fn increases. Conversely, when incorporating all attachments, both experimental and simulation data exhibit a trend towards a subtle increase in bow trim up to approximately Fn = 0.2. Significant fluctuations in the experimental data are noted, due to a variety of measurement factors or scale effects. It can be observed that the simulations tend to under-estimate the values by approximately 20% on average compared to those measured experimentally. For Fns greater than 0.2, where experimental data are absent, a gradual decrease in bow trim is observed, underscoring the need for additional experimental investigation in higher Fn ranges. Next, in the analysis of sinkage, both experiments and CFD simulations show minimal overall changes. Nevertheless, the CFD results, when considering all attachments, indicate a slight increase in settlement for Fn < 0.2, similar to the experiment, followed by a decreasing trend above this range.

In summary, the running trim of a vessel is subtly influenced by the type of attachment affixed. Specifically, a vessel outfitted with all attachments exhibits a bow trim at Fn below 0.22, with a minor tendency towards buoyancy. This pattern, however, reverses at Fn greater than 0.22, highlighting a complicated interaction between the running trim and the appendages attached. This phenomenon warrants further investigation to fully understand the dynamics at play.

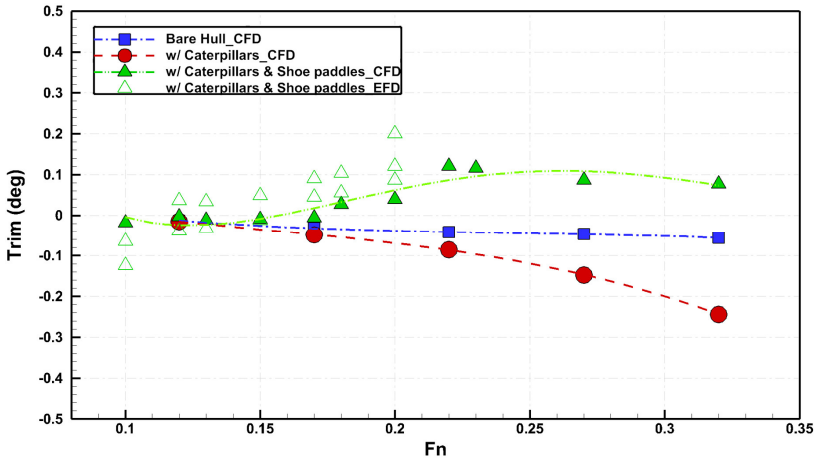

Figure 15. Results of trim as a function of Froude number.

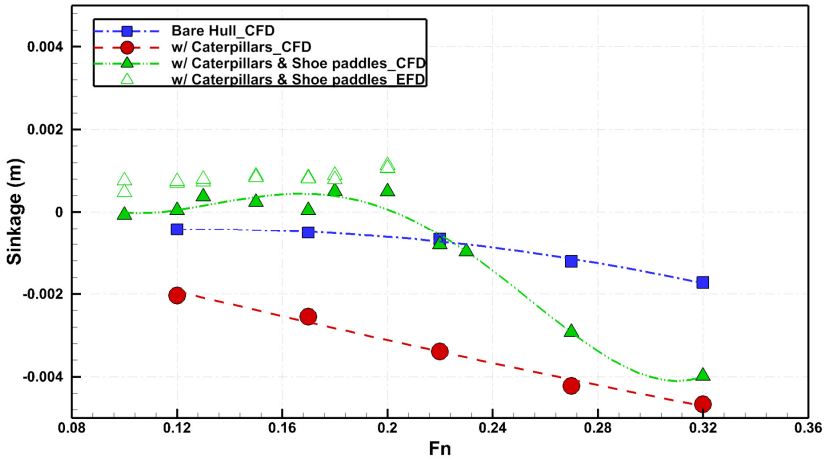

Figure 16. Results of sinkage as a function of Froude number.

4. Conclusions

In this study, the resistance performance of an amphibious vessel utilized for marine debris collection, equipped with and without caterpillars and shoe−paddles, was analyzed through CFD simulation and substantiated by a model tested in a wave tank with a towing carriage. The present study led to the following conclusions:

- The accuracy of the CFD simulation was confirmed, with a total resistance error margin of less than 6.6% when compared to the model tests. Furthermore, an evaluation of resistance at varying speeds of the vessel revealed a considerable influence of the attachments on total resistance. Notably, at the design speed (Fn = 0.27), the resistance of the configuration with both caterpillars and shoe−paddles was 75.7% higher than that of the bare hull and 11.0% more than that with caterpillars alone.
- When dividing the total resistance into pressure and friction components at the design speed, it was indicated that pressure resistance constitutes the major portion of the total resistance across all configurations. It accounted for 84.3% of the total resistance in the bare hull configuration, 91.6% with caterpillars, and 92.0% with both caterpillars and shoe−paddles.
- This study examined the influence of attachments on wave dynamics around the vessel. Incorporating caterpillars and shoe−paddles led to the formation of more distinct wave patterns around the vessel, with significant wave propagation observed in the far field. These attachments served to dampen wave generation in the vicinity of the vessel through wave-breaking phenomena, resulting in reduced wave activity and a more quiescent flow aft.

The insights derived from this study are anticipated to contribute valuable information to the ongoing research and development process of amphibious vessels, particularly those designated for marine debris collection.

Author Contributions: Conceptualization J.-C.P.; methodology, W.-J.J.; experiment, H.K.Y.; software, W.-J.J.; validation, W.-J.J.; formal analysis, W.-J.J.; investigation, W.-J.J. and S.N.; resources, W.-J.J. and H.K.Y.; data curation, W.-J.J.; writing—original draft preparation, W.-J.J. and S.N.; writing—review and editing, J.-C.P.; visualization, W.-J.J.; supervision, J.-C.P.; project administration, J.-C.P. All authors have read and agreed to the published version of the manuscript.

Funding: This research was a part of the project titled 'Development of coastal garbage collection technology in difficult-to-access areas', funded by the Ministry of Oceans and Fisheries, South Korea (20200584).

Institutional Review Board Statement: Not applicable

Informed Consent Statement: Not applicable

Data Availability Statement: Not applicable.

Conflicts of Interest: The authors declare no conflicts of interest.

References

1. UNEP. *Report of the United Nations Environment Assembly of the United Nations Environment Programme (Nairobi, 23–27 June 2014)*; UN Doc A/69/25; UN: New York, NY, USA, 2014.
2. Nakisa, M.; Maimun, A.; Ahmed, Y.M.; Behrouzi, F.; Tarmizi, A. Numerical estimation of shallow water effect on multipurpose amphibious vehicle resistance. *J. Nav. Archit. Mar. Eng.* **2017**, *14*, 1–8.
3. Yamashita, H.; Arnold, A.; Carrica, P.M.; Noack, R.W.; Martin, J.E.; Sugiyama, H.; Harwood, C. Coupled Multibody Dynamics and Computational Fluid Dynamics Approach for Amphibious Vehicles in the Surf Zone. *Ocean. Eng.* **2022**, *257*, 111607.
4. Sun, C.; Xu, X.; Wang, W.; Xu, H. Influence on stern flaps in resistance performance of a caterpillar track amphibious vehicle. *IEEE Access* **2020**, *8*, 123828–123840.
5. Pan, D.; Xu, X.; Liu, B. Influence of flanks on resistance performance of high-speed amphibious vehicle. *J. Mar. Sci. Eng.* **2021**, *9*, 1260.
6. Liu, B.; Xu, X.; Pan, D. Resistance reduction optimization of an amphibious transport vehicle. *Ocean Eng.* **2023**, *280*, 114854.
7. Jaouad, H.; Vikram, P.; Balasubramanian, E.; Surendar, G. Computational Fluid Dynamic Analysis of Amphibious Vehicle. In *Advances in Engineering Design and Simulation*; Springer: Berlin, Germany, 2020; pp. 303–313.
8. More, R.R.; Adhav, P.; Senthilkumar, K.; Trikande, M.W. Stability and drag analysis of wheeled amphibious vehicle using CFD and model testing techniques. *Appl. Mech. Mater.* **2014**, *592*, 1210–1219.
9. Guo, Z.; Pan, Y.; Zhang, H.; Wang, Y. Numerical simulation of an amphibious vehicle sailing resistance. *Int. J. Comput. Sci. Issues (IJCSI)* **2013**, *10*, 33.
10. Pan, X.; Yao, K.; Duan, L.; Hou, Z.; Tian, X.; Zhao, X. Simulation of Amphibious Vehicle Water Resistance Based on FLUENT. In Proceedings of the 2015 International Conference on Materials Engineering and Information Technology Applications, Guilin, China, 30–31 August 2015; pp. 485–489.
11. Du, Z.; Mu, X.; Zhu, H.; Han, M. Identification of Critical Parameters Influencing Resistance Performance of Amphibious Vehicles Based on a SM-SA Method. *Ocean Eng.* **2022**, *258*, 111770.
12. Behara, S.; Arnold, A.; Martin, J.E.; Harwood, C.M.; Carrica, P.M. Experimental and computational study of operation of an amphibious craft in calm water. *Ocean Eng.* **2020**, *209*, 107460.
13. Lee, S.J.; Lee, T.I.; Lee, J.J.; Nam, W.; Suh, J.C. Hydrodynamic characteristics of a hydrofoil-assisted amphibious vehicle. *J. Ship Res.* **2017**, *61*, 15–22.
14. Dhana, F.R.; Park, J.C.; Yoon, H.K. A Numerical Study on the Influence of Caterpillars to the Resistance Performance of an Amphibious Vehicle. *J. Mar. Sci. Eng.* **2023**, *11*, 286.
15. Youn, T.G.; Kim, M.J.; Kim, M.C.; Kang, J.G. Effect of Free Surface Based on Submergence Depth of Underwater Vehicle. *J. Ocean. Eng. Technol.* **2022**, *36*, 83–90.
16. Simcenter STAR-CCM+ Version 2022.1, News Part 1—Multiphase—Volupe Software. Available online: https://volupe.se/en/simcenter-star-ccm-version-2022-1-news-part-1-multiphase/ (accessed on 30 December 2022).
17. ITTC. *ITTC—Practical Guidelines for Ship CFD Applications*; ITTC: Singapore, 2011.
18. Rakowitz, M. Grid Refinement Study with a Uhca Wing-Body Configuration Using Richardson Extrapolation and Grid Convergence Index Gci. In *New Results in Numerical and Experimental Fluid Mechanics III*; Springer: Heidelberg, Germany, 2002; pp. 297–303.
19. Roache, P.J. Perspective: A method for uniform reporting of grid refinement studies. *J. Fluids Eng.* **1994**, *116*, 405–413.
20. Roache, P.J. Quantification of uncertainty in computational fluid dynamics. *Annu. Rev. Fluid Mech.* **1997**, *29*, 123–160.

21. Choi, H.S.; Kwon, S.Y.; Kim, S.H.; Kim, I.T. Study on the Manoeuvring Performance of a Fishing Vessel Based on CFD Simulation of the Hull Forms and Rudder Shapes. *J. Ocean Eng. Technol.* **2023**, *37*, 129–136.
22. Kristensen, H.O.; Lützen, M. *Prediction of Resistance and Propulsion Power of Ships*; Project no. 2010-56, Emissionsbeslutningsstøttesystem Work Package 2, Report no. 04 May 2013; Technical University of Denmark: Kongens Lyngby, Denmark; University of Southern Denmark: Odense, Denmark, 2013; pp. 4–11.